Supplement for manuscript

Influence of Intense secondary aerosol formation and long range transport on aerosol chemistry and properties in the Seoul Metropolitan Area during spring time: Results from KORUS-AQ

Hwajin Kim[1,2] ,Qi Zhang[3,4*] and Jongbae Heo[5]

[1] Center for Environment, Health and Welfare Research, Korea Institute of Science and Technology, Seoul, Korea

[2] Department of Energy and Environmental Engineering, University of Science and Technology, Daejeon, Korea

[3] Department of Environmental Science and Engineering, Fudan University, Shanghai, China.

[4] Department of Environmental Toxicology, University of California, Davis, CA 95616, USA

[5] Center for Healthy Environment Education & Research, Graduate School of Public Health, Seoul National University, Seoul, Korea

*Corresponding author: Qi Zhang

Department of Environmental Toxicology, University of California 1 Shields Avenue, Davis, California 95616

Phone: (530)-752-5779

Email: dkwzhang@ucdavis.edu

Table S1. Comparison of the average O/C, H/C, and OM/OC ratios of total OA and the four OA factors identified from PMF analysis calculated using the Aiken-Ambient method (Aiken et al., 2008) and the improved Canagaratna-Ambient method (Canagaratna et al., 2015).

Species	Ratio	Aiken-Ambient	Canagaratna-Ambient
OA	O/C	0.38	0.49
	H/C	1.52	1.67
	OM/OC	1.66	1.82
HOA	O/C	0.11	0.15
	H/C	1.85	2.00
	OM/OC	1.31	1.37
COA	O/C	0.15	0.19
	H/C	1.68	1.83
	OM/OC	1.34	1.41
SVOOA	O/C	0.33	0.44
	H/C	1.55	1.73
	OM/OC	1.58	1.74
LVOOA	O/C	0.51	0.91
	H/C	1.41	1.46
	OM/OC	1.84	2.36

Table S2. Comparison of aerosol properties and meteorological parameters at different stages during haze period.

	Overall	**S1**	**S2**	**S3**	**S4**
Average non-refractory submicrometer particulate matter (NR-PM_1) mass concentration ($\mu g\ m^{-3}$) (Average)	22.1	9.0	41.2	37.7	13.0
RH(%) / Temp(°C)	62/19	96/16	78/18	67/21	48/23
WS(m/s)	1.7	3.0	2.2	1.4	1.7
Trace gas conc.(CO (ppm) and /SO_2/ NO_2 O_3/(ppb))	0.52/5.1/34/ 29	0.48/4.0/39/ 15	0.55/4.8/32/ 39	0.62/6.1/37/ 35	0.39/4.5/28.7 /33

PM, particulate matter; NR-PM_1, non-refractory submicrometer particulate matter; RH, relative humidity

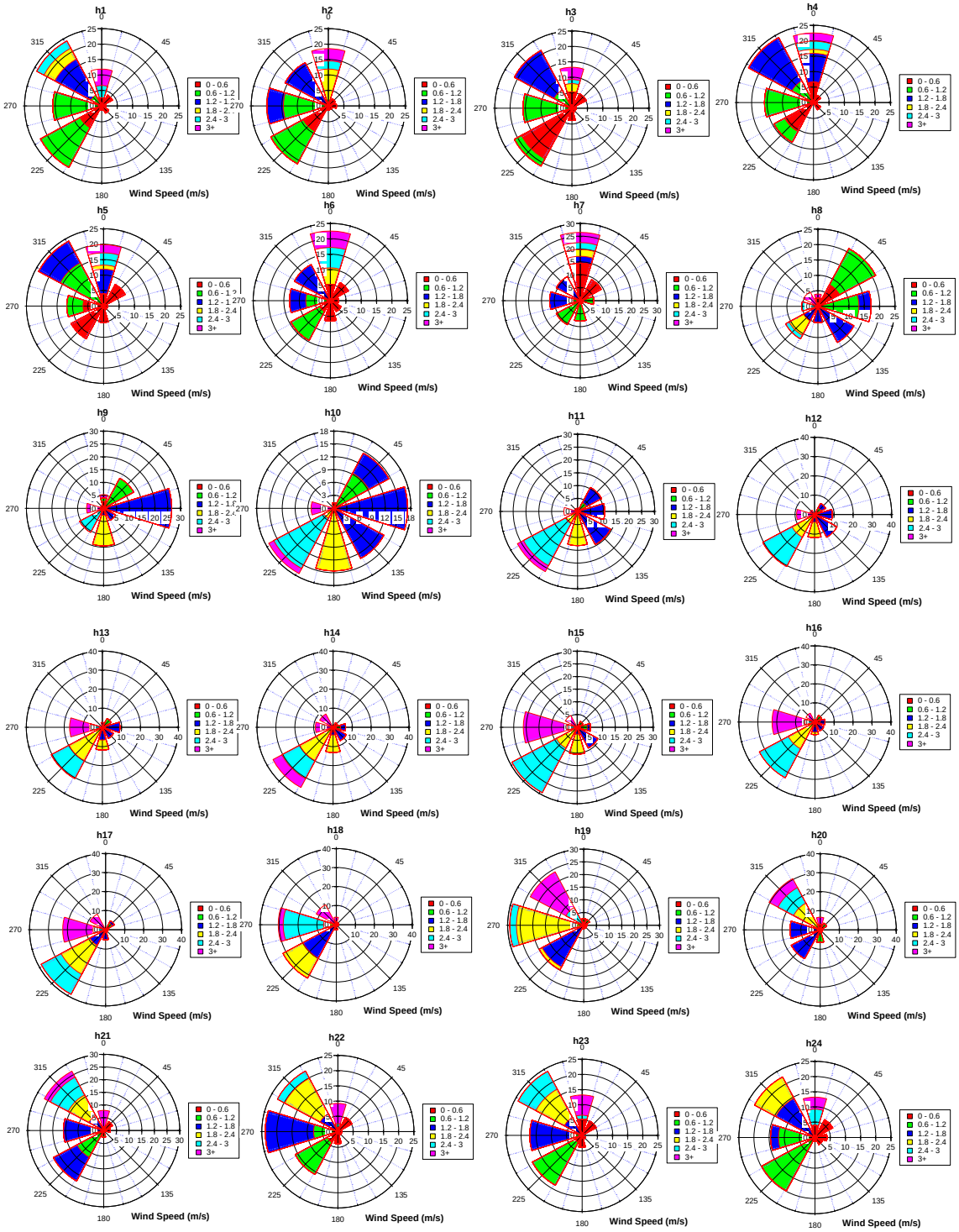

Figure S1. Wind Rose plots for every hour colored by wind speed. Radial scales correspond to the frequency.

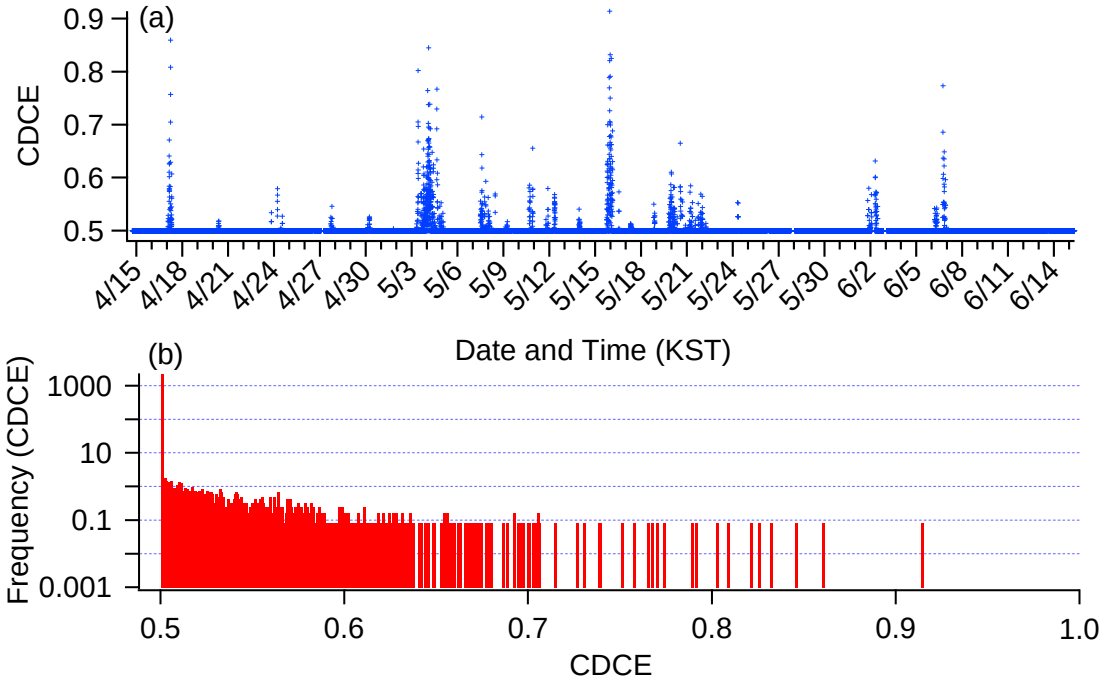

Figure S2. (a) Time series of composition dependent collection efficiency (CDCE) and; **(b)** histogram of CDCE, averaging 0.5 ± 0.01.

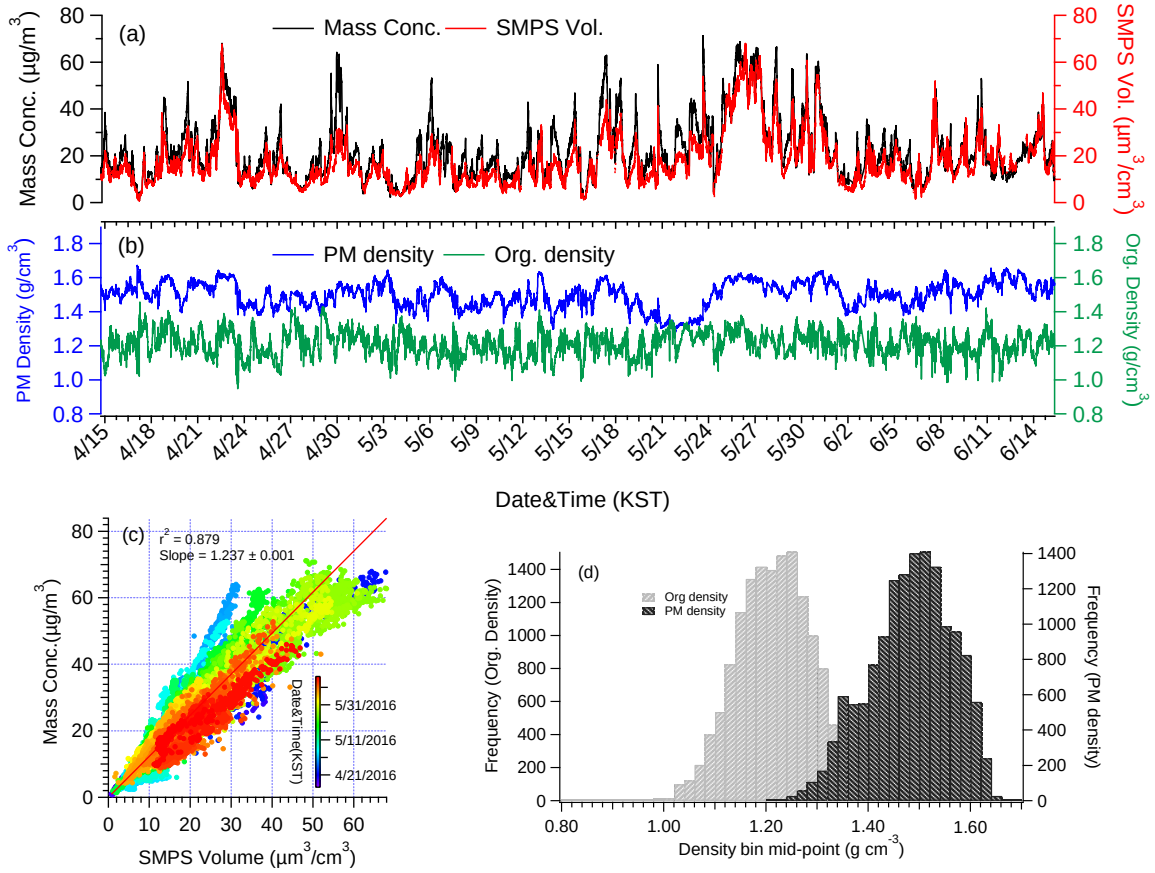

Figure S3. (a) Time series of total particulate matter (PM_1), scanning mobility particle sizer (SMPS) volume concentrations ; **(b)** Time series of the organic aerosol density estimated using the method reported in Kuwata et al. (2012)

$$\rho_{org} = [12 + 1\bullet(H/C) + 16\bullet(O/C)]/ [7 + 5\bullet(H/C) + 4.15\bullet(O/C)]$$

and bulk aerosol density estimated from the measured chemical composition, known inorganic species density and the organic density estimated above (Zhang et al., 2005). **(c)** Scatter plot of the total PM_1 mass (NR-PM_1 plus BC) versus SMPS volume, where the NR-PM_1 mass concentrations have been determined using the composition-dependent collection efficiencies; **(d)** histogram of organic aerosol density (average = 1.21 g cm^{-3}) and bulk aerosol density (average = 1.5 g cm^{-3}).

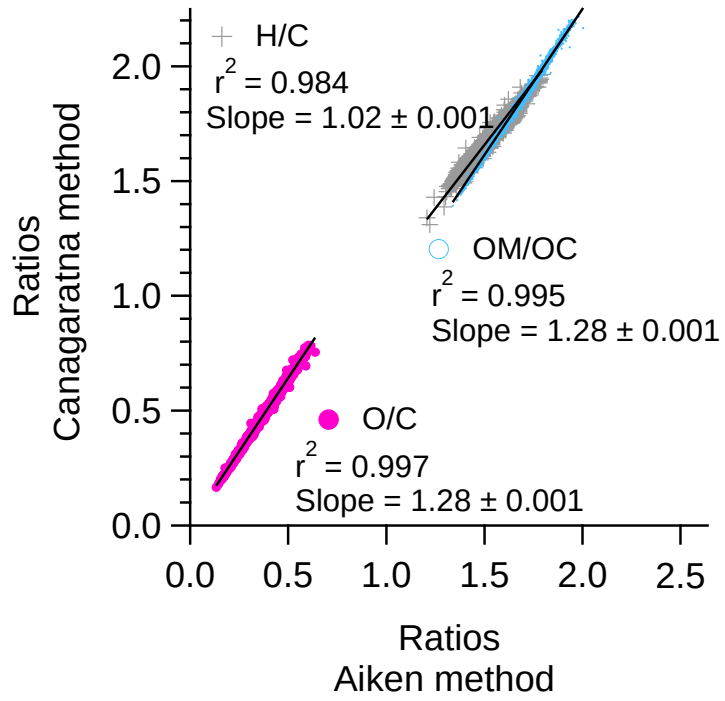

Figure S4. Scatter plot of OM/OC, O/C, and H/C calculated with the Canagaratna method vs. those with the Aiken-Ambient method.

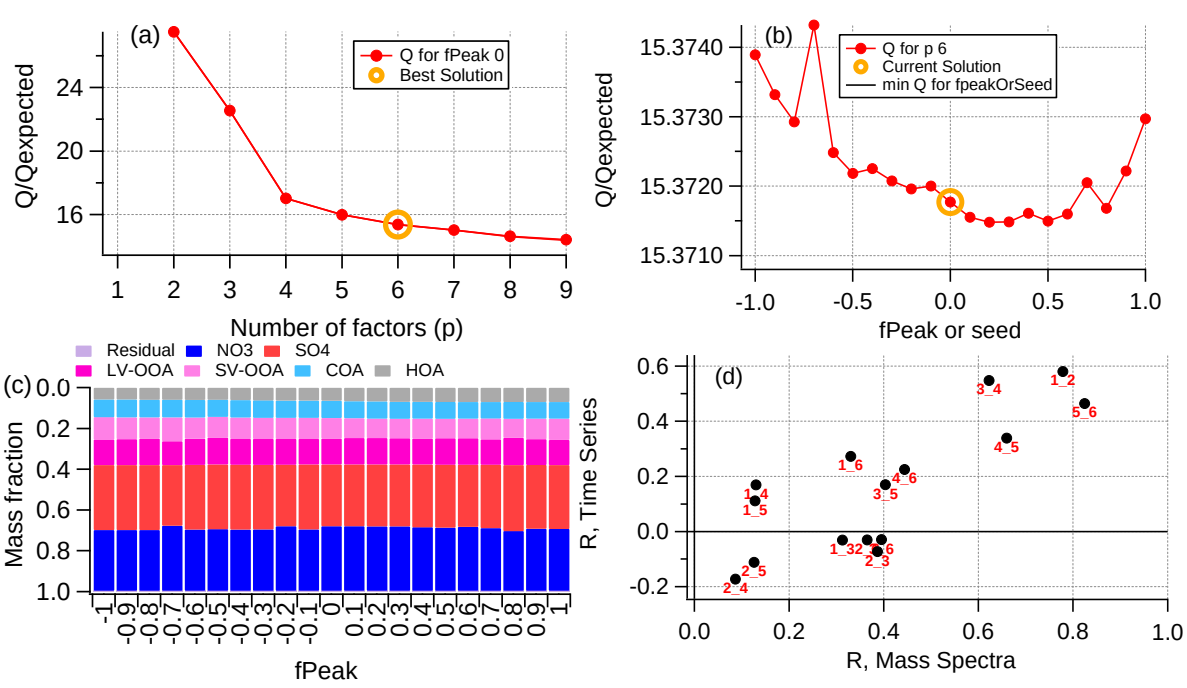
(a)
Q for fPeak 0
Best Solution
Q/Qexpected
Number of factors (p)
(b)
Q for p 6
Current Solution
min Q for fpeakOrSeed
Q/Qexpected
fPeak or seed
(c)
Residual
NO3
SO4
LV-OOA
SV-OOA
COA
HOA
Mass fraction
fPeak
(d)
R, Time Series
R, Mass Spectra

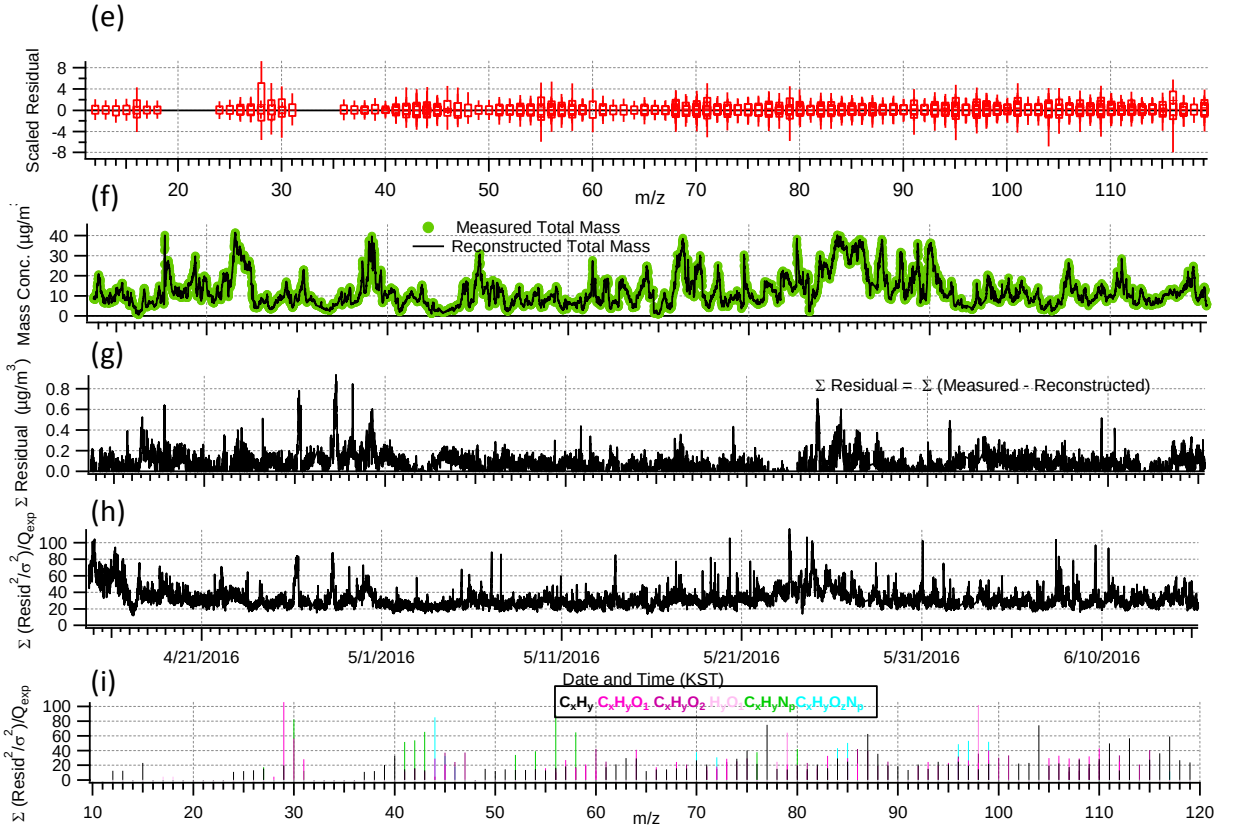
(e)
Scaled Residual
m/z
(f)
Measured Total Mass
Reconstructed Total Mass
Mass Conc. (µg/m
(g)
Σ Residual = Σ (Measured - Reconstructed)
Σ Residual (µg/m3)
(h)
Σ (Resid2/σ2)/Qexp
4/21/2016
5/1/2016
5/11/2016
5/21/2016
5/31/2016
6/10/2016
Date and Time (KST)
(i)
CxHy CxHyO1 CxHyO2 HyO3 CxHyNp CxHyO2Np
m/z

147

148 **Figure S5.** Summary of the key diagnostic plots of the chosen 6-factor solution (4 OA factor
149 solution) from PMF analysis of the organic aerosol fraction: **(a)** Q/Q_{exp} as a function of the number
150 of factors (*p*) explored in PMF analysis, with the best solution denoted by the open orange circle.
151 Plots **b-i** are for the chosen solution set, containing 4 factors: **(b)** Q/Q_{exp} as a function of fPeak; **(c)**
152 mass fractional contribution to the total mass of each of the PMF factors, including the residual (in
153 purple), as a function of fPeak; **(d)** Pearson's r correlation coefficient values for correlations among
154 the time series and mass spectra of the PMF factors. Here, 1 = NO_3, 2 = SO_4, 3 = LV-OOA, 4 =
155 SV-OOA, 5 = COA, 6 = HOA; **(e)** box and whiskers plot showing the distributions of scaled
156 residuals for each *m/z*; **(f)** time series of the measured mass and the reconstructed mass from the
157 sum of the 6 factors; **(g)** time series of the variations in the residual (= measured – reconstructed)
158 of the fit; **(h)** the Q/Q_{exp} for each point in time; **(i)** the Q/Q_{exp} values for each fragment ion.

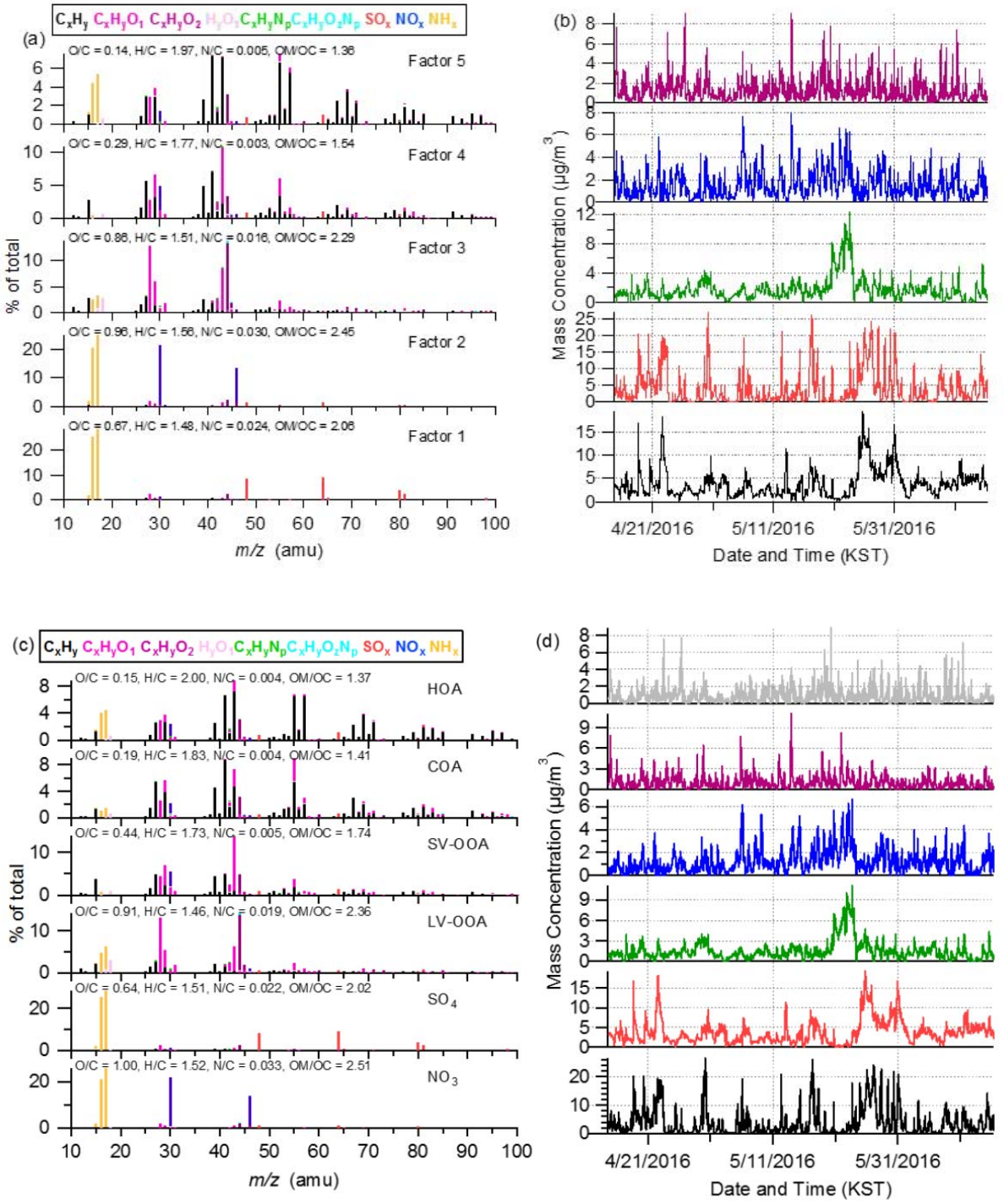
(a)
CxHy CxHyO1 CxHyO2 HyOz CxHyNp CxHyOzNp SOx NOx NHx
O/C = 0.14, H/C = 1.97, N/C = 0.005, OM/OC = 1.36
Factor 5
O/C = 0.29, H/C = 1.77, N/C = 0.003, OM/OC = 1.54
Factor 4
O/C = 0.86, H/C = 1.51, N/C = 0.016, OM/OC = 2.29
Factor 3
O/C = 0.96, H/C = 1.56, N/C = 0.030, OM/OC = 2.45
Factor 2
O/C = 0.67, H/C = 1.48, N/C = 0.024, OM/OC = 2.06
Factor 1
% of total
m/z (amu)
(b)
Mass Concentration (μg/m3)
4/21/2016
5/11/2016
5/31/2016
Date and Time (KST)
(c)
CxHy CxHyO1 CxHyO2 HyOz CxHyNp CxHyOzNp SOx NOx NHx
O/C = 0.15, H/C = 2.00, N/C = 0.004, OM/OC = 1.37
HOA
O/C = 0.19, H/C = 1.83, N/C = 0.004, OM/OC = 1.41
COA
O/C = 0.44, H/C = 1.73, N/C = 0.005, OM/OC = 1.74
SV-OOA
O/C = 0.91, H/C = 1.46, N/C = 0.019, OM/OC = 2.36
LV-OOA
O/C = 0.64, H/C = 1.51, N/C = 0.022, OM/OC = 2.02
SO4
O/C = 1.00, H/C = 1.52, N/C = 0.033, OM/OC = 2.51
NO3
% of total
m/z (amu)
(d)
Mass Concentration (μg/m3)
4/21/2016
5/11/2016
5/31/2016
Date and Time (KST)

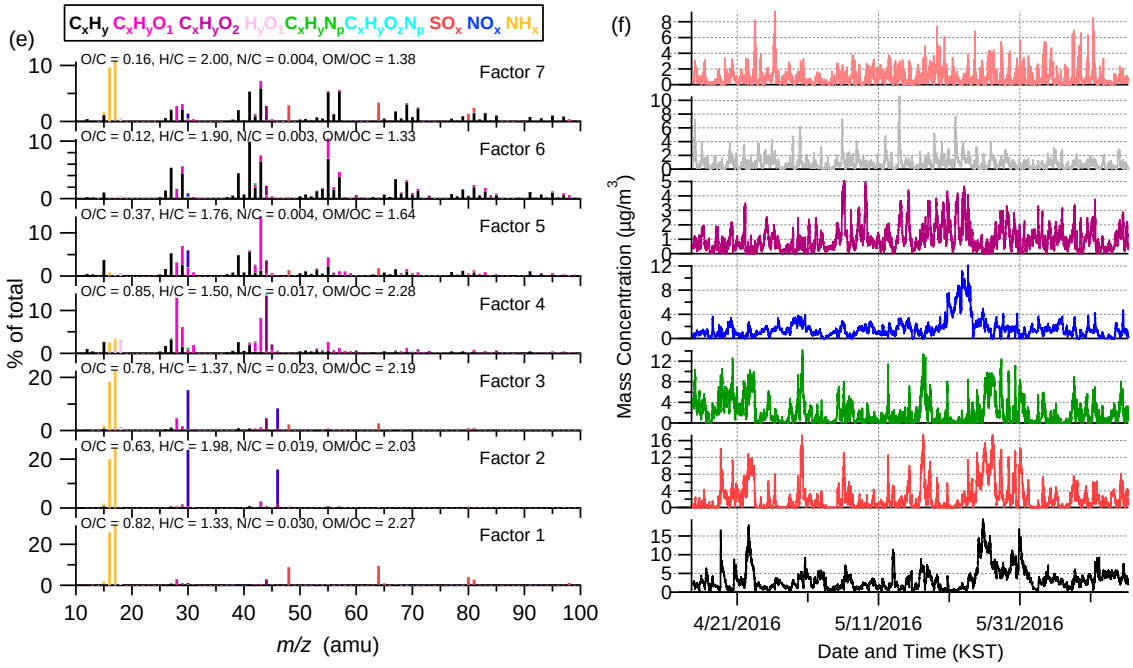

Figure S6. Overview of two other solution sets and 6-factor solution including inorganic factors and signals from inorganic included PMF analysis: **(a)(b)** High resolution mass spectra and time series of the different OA factors from the 5-factor solution (3-OA); **(c)(d)** High resolution mass spectra and time series of the different OA factors from the 6-factor solution (4-OA); **(e)(f)** High resolution mass spectra and time series of the different OA factors from the 7-factor solution (5-OA). The mass spectra are colored by different ion families.

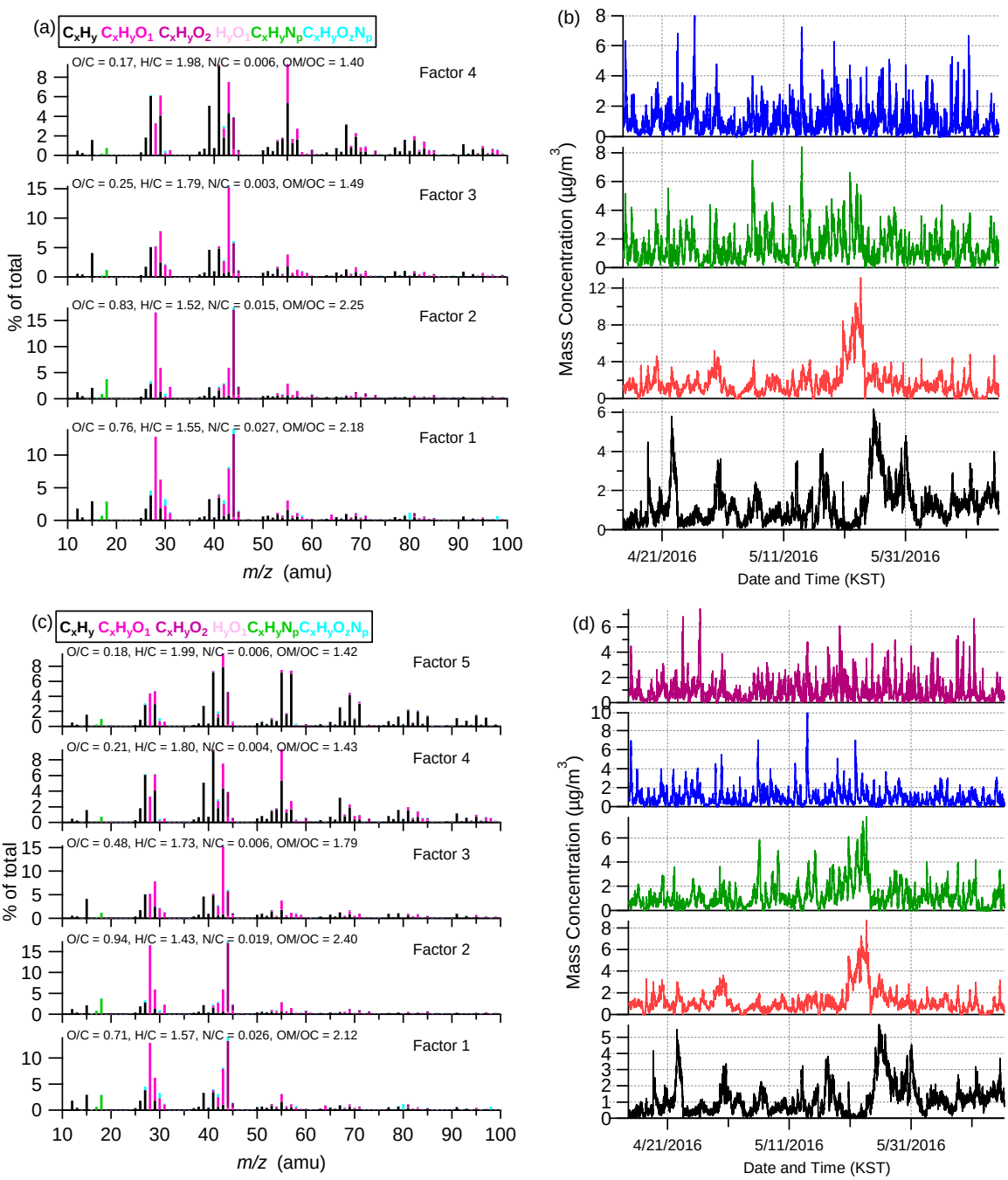

Figure S7. Overview of the 4-factor solution (**a** and **b**) and the 5-factor solution (**c** and **d**) from PMF analysis of the organic mass spectra only. The mass spectra are colored by different ion families.

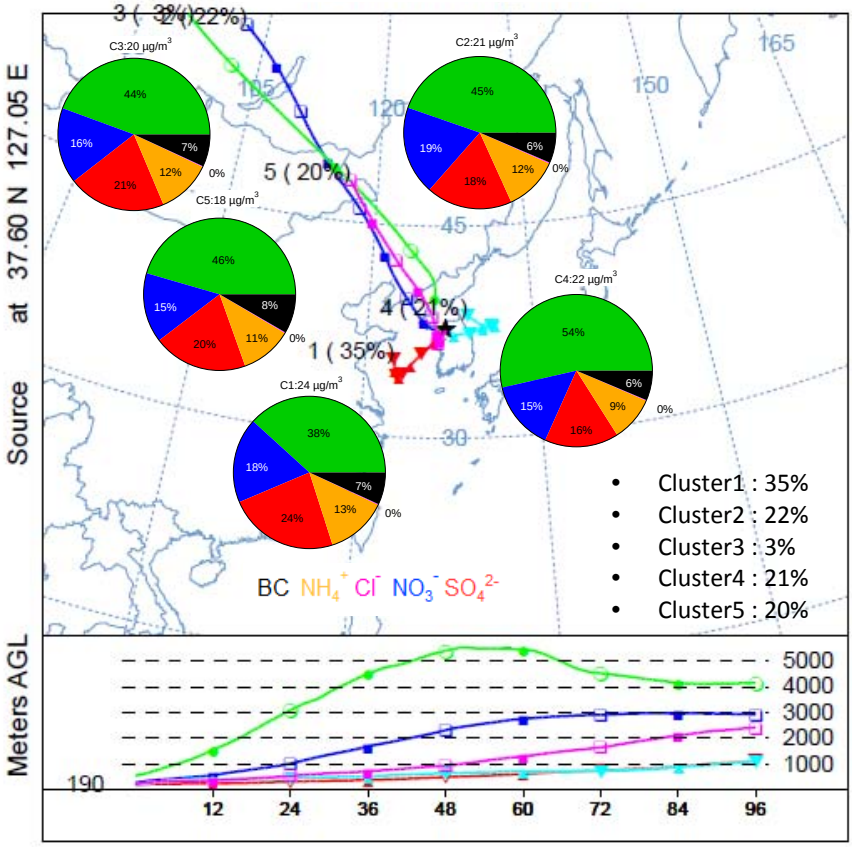

Figure S8. Averaged compositional pie chart of PM_1 species (non-refractory-PM_1 plus black carbon (BC)) in different clusters from the five cluster solution. The trajectories were released at half of the mixing height at the KIST (latitude: 37.60N; longitude: 127.05E) and the average arriving height for the back trajectories for this study was approximately 190 m.

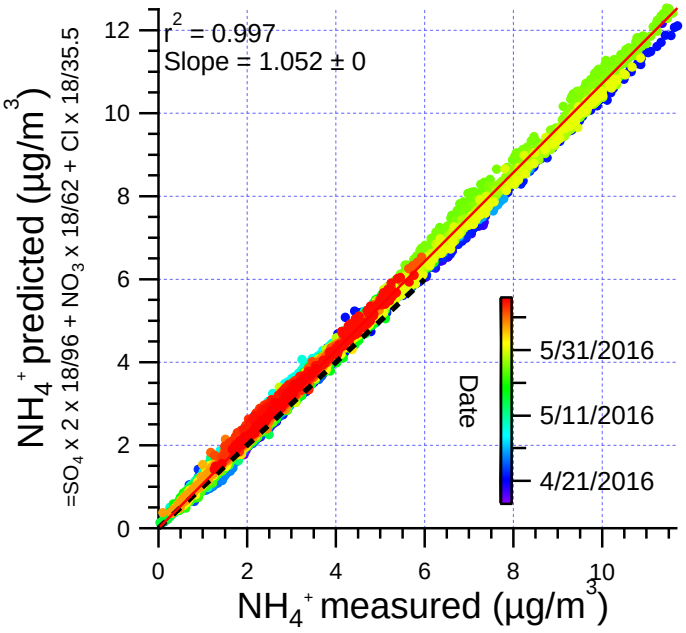

Figure S9. Scatterplot that compares predicted NH_4^+ versus measured NH_4^+ concentrations. The predicted values were calculated assuming full neutralization of the anions (e.g., sulfate, nitrate, and chloride). The data points are colored by date.

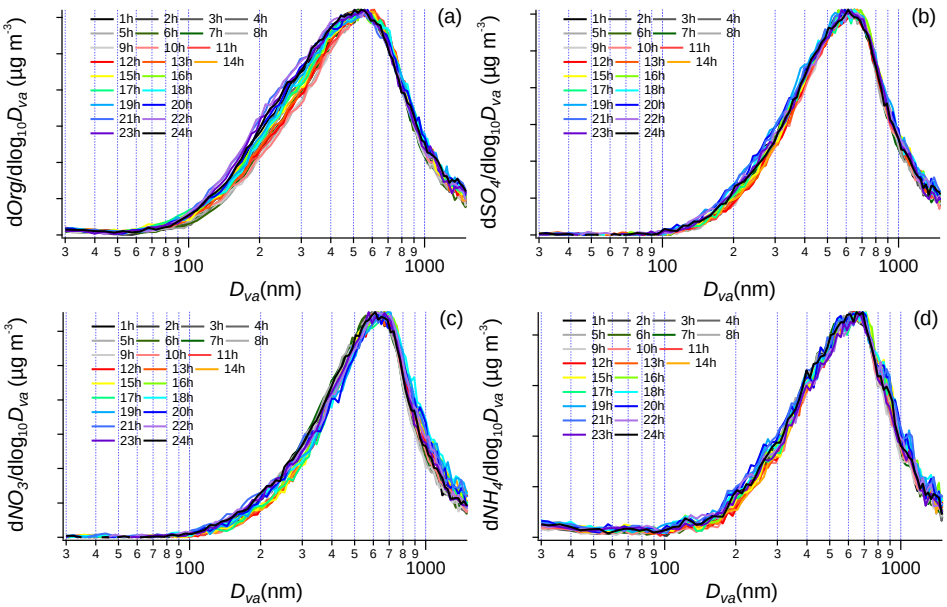

Figure S10. Size distributions for (a) organic; (b) Sulfate: (c) Nitrate; (d) ammonium for every hour. Y axis are shared for all distributions which are maximized to the axis.

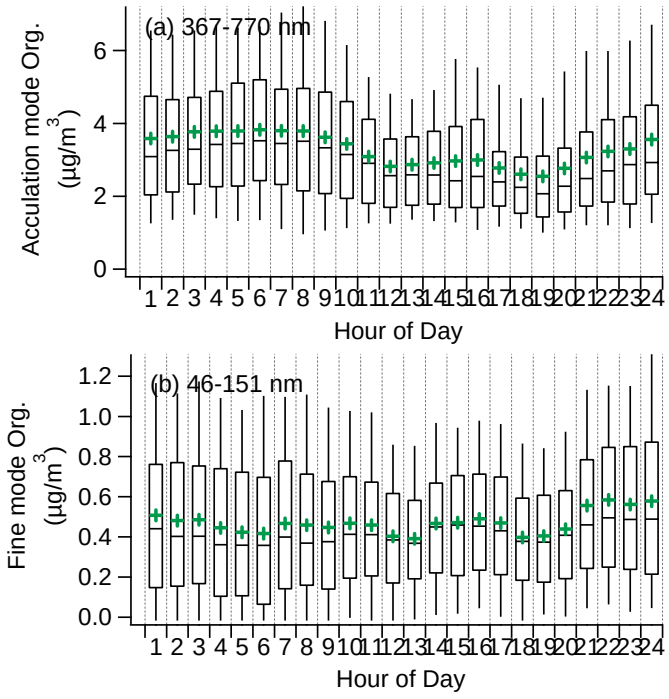

Figure S11. One-hour averaged diurnal profiles of organics in (a) accumulation mode and (b) fine mode.

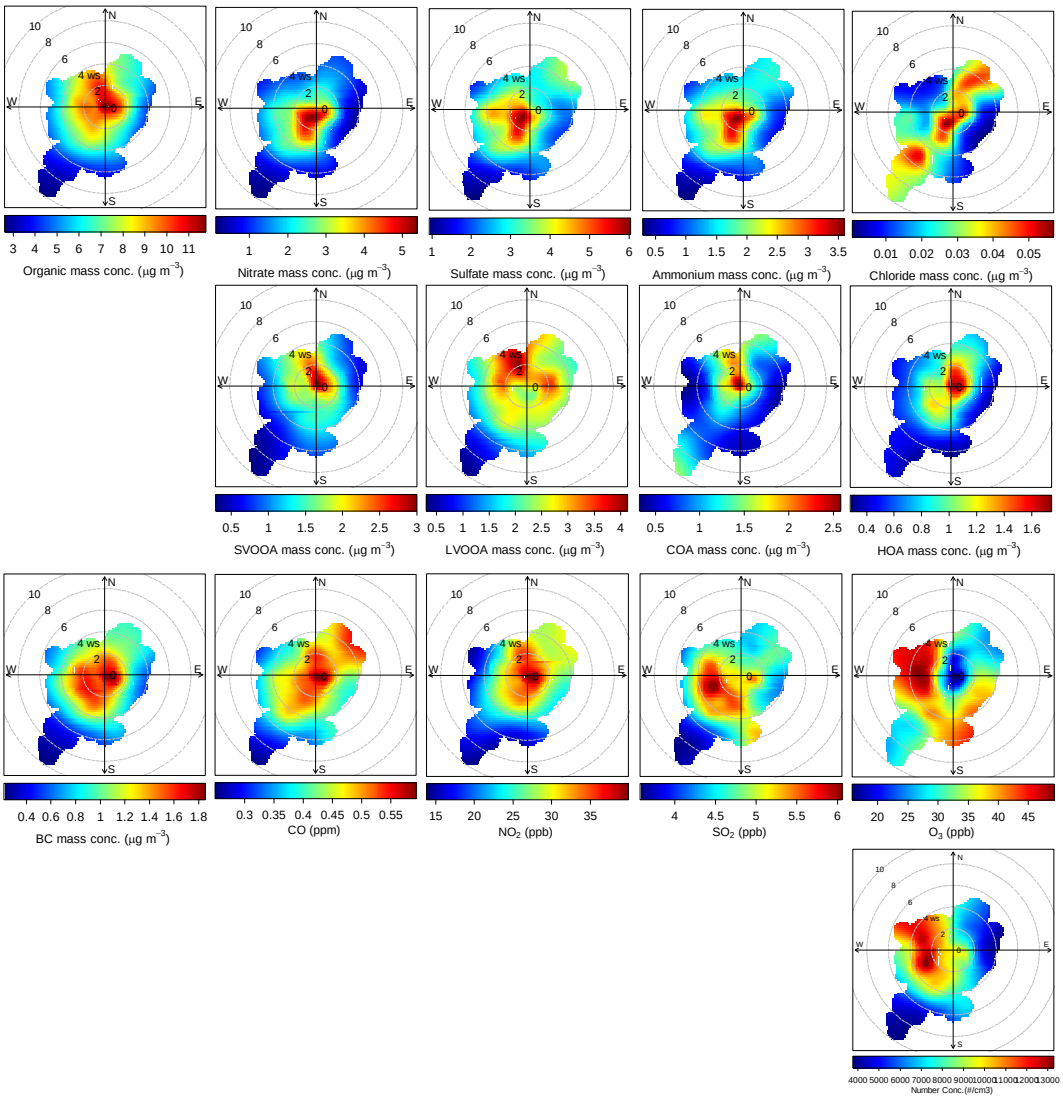

Figure S12. Polar plots of hourly averaged PM_1 species concentrations (top row), mass concentrations of the five OA factors identified from PMF analysis (middle row), the mixing ratios of various gas phase species (second row from the bottom), and the particle number concentrations (bottom row) as a function of WS and direction.

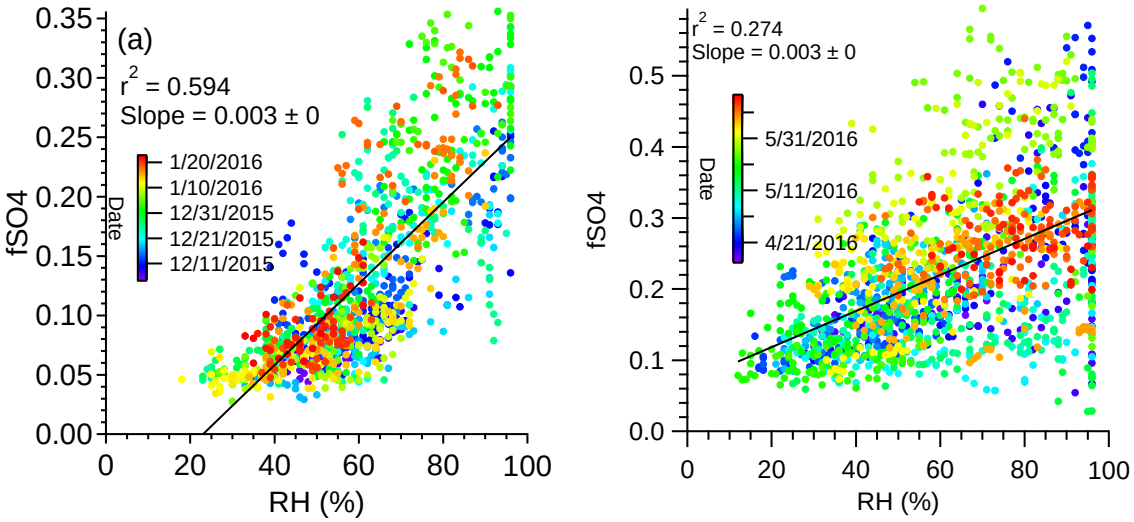

Figure S13. Scatterplot of the variations of fSO_4 ratios as a function of RH **(a)** during winter (Kim et al., 2017); **(b)** during spring in this study.

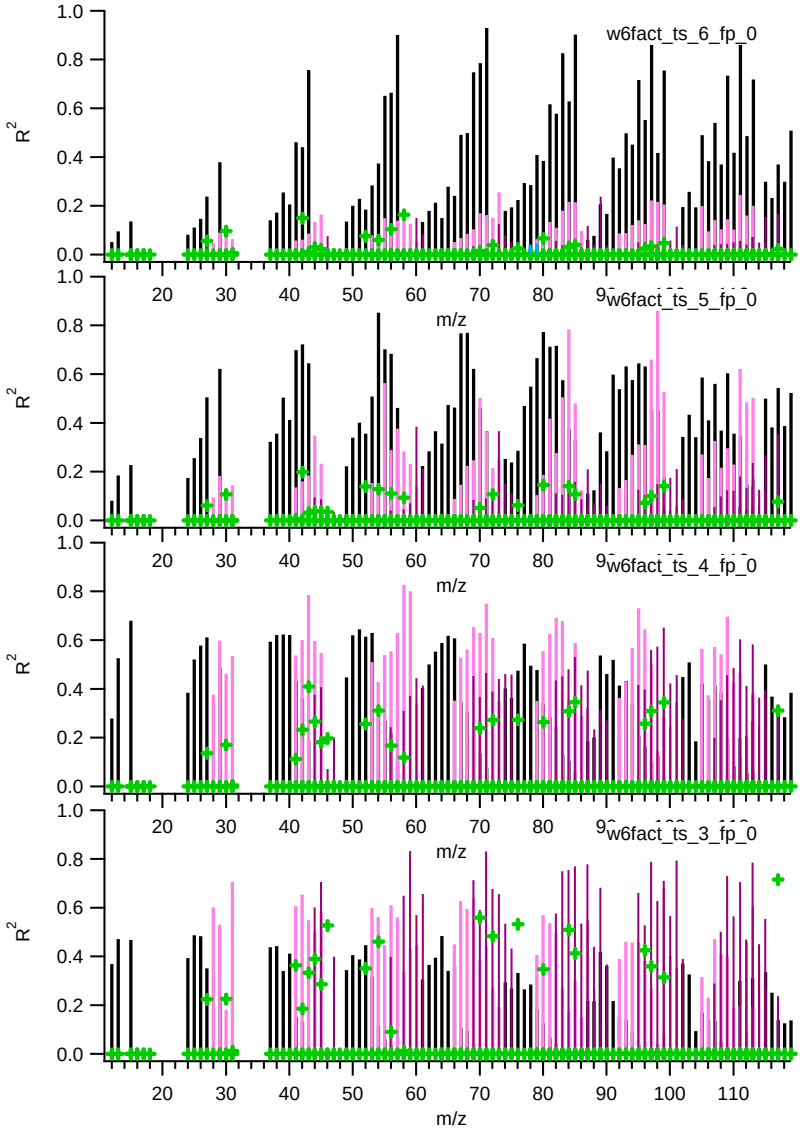

Figure S14. Correlations between four OA factors and HRMS ions that are segregated into five categories ($C_xH_y^+$, $C_xH_yO^+$, $C_xH_yO_2^+$, $C_xH_yN_p^+$ and $C_xH_yO_zS_q^+$).From the top, HOA, COA, SV-OOA and LV-OOA.

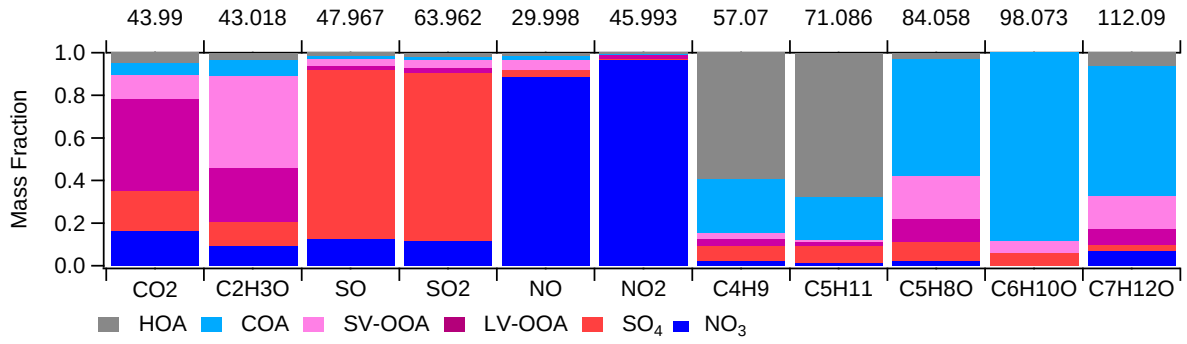

365

366

367 **Figure S15.** Mass fractional contribution of the factors (four OA factors + two inorganic factors)
368 from PMF analysis to various ions that are relevant to each significant tracer.

369

370

371

372

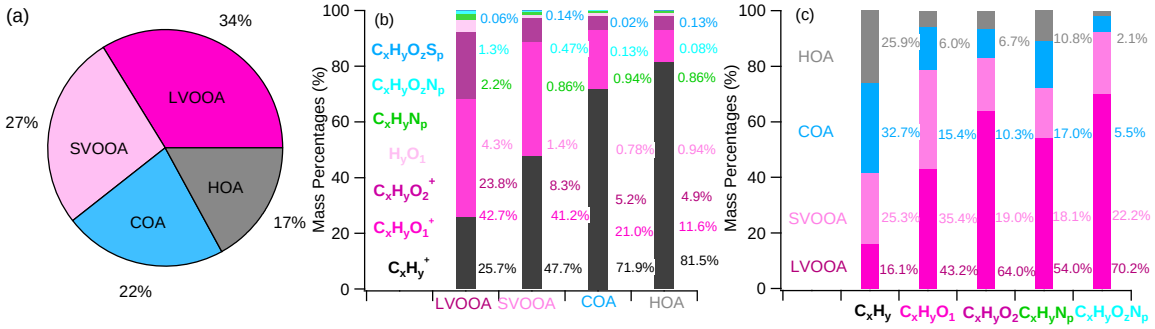

373 **Figure S16. (a)** Compositional pie chart of the average fractional contribution of each of the OA
374 factors to the total OA over the campaign; **(b)** Average mass fractional contributions of seven ion
375 families to each of the OA factors and; **(c)** Average mass fractional contributions of four OA
376 factors to 4 each ion families

377

378

379

380

381

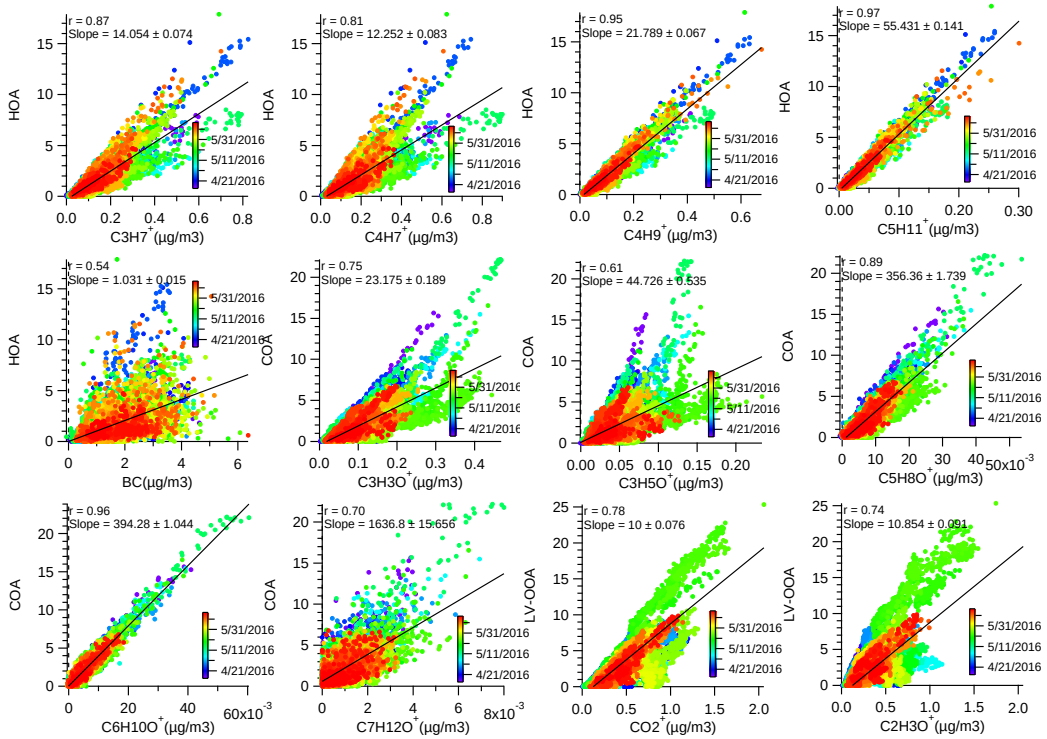

Figure S17. Scatter plots of factors and relevant tracer ions colored by measurement date.

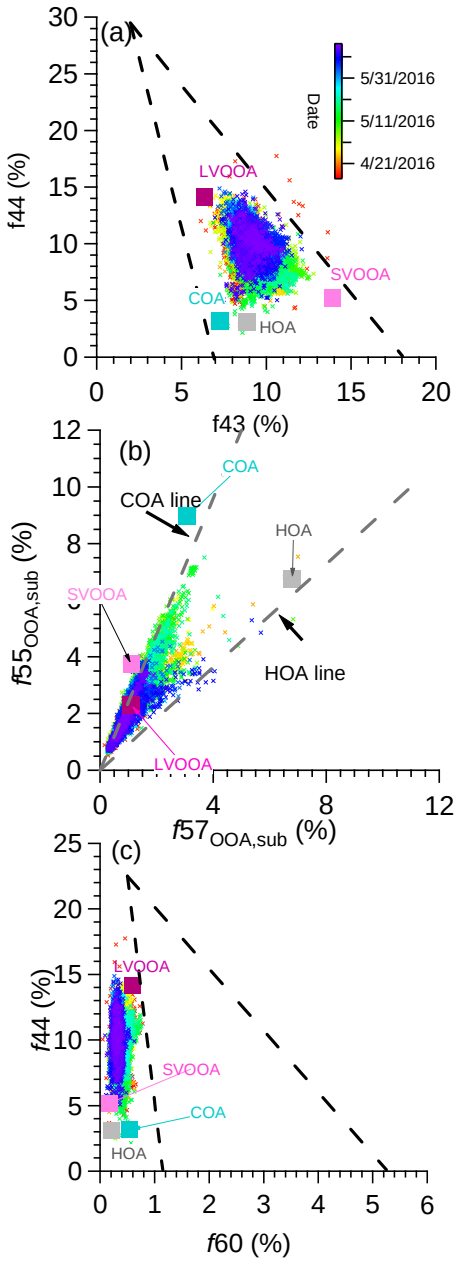

Figure S18. Triangular plots of **(a)** f_{44} versus f_{43} and **(b)** f_{44} versus f_{60} (c) $f_{55,\mathrm{OOA\ sub}}$ versus $f_{57,\mathrm{OOA\ sub}}$ for the five OA factors and all of the measured OA data (dots), colored by the time of the day. f_{43}, f_{44}, and f_{60} are the ratios of the organic signal at m/z = 43, 44, and 60 to the total organic signal in the component mass spectrum, respectively. $f_{55,\mathrm{OOA\ sub}}$ and $f_{55,\mathrm{OOA\ sub}}$ are the ratios of the organic signal at m/z 55, 57 after subtracting the contributions from SV-OOA and LV-OOA (e.g., $f_{55,\mathrm{OOA\ sub}} = m/z\ 55 - m/z55_{SV\text{-}OOA} - m/z55_{LV\text{-}OOA}$; $f_{57,\mathrm{OOA\ sub}} = m/z\ 57 - m/z\ 57_{SV\text{-}OOA} - m/z\ 57_{LV\text{-}OOA}$)

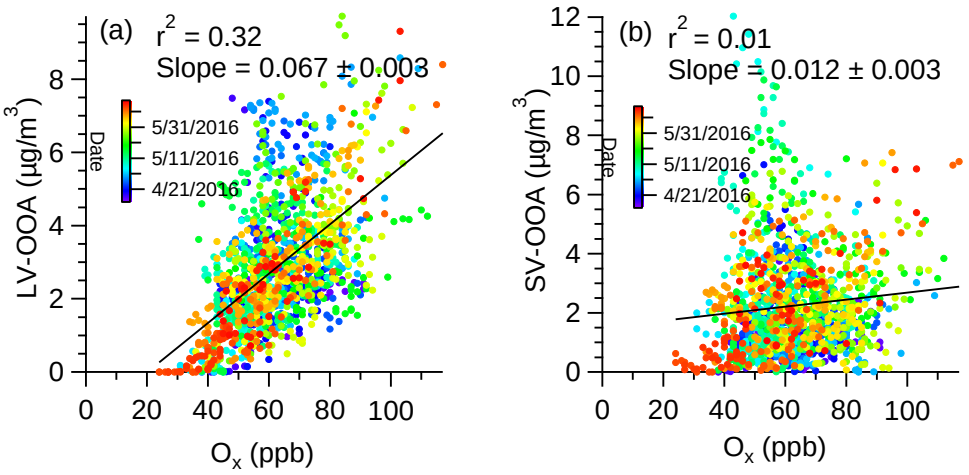

Figure S19. Scatter plots of **(a)** LV-OOA vs. O_x; **(b)** SV-OOA vs O_x over the entire period in the spring. Note that organic dominant period (5/20, 17:00 - 5/24, 0:00) are excluded. All scatter plots are colored by measurement date.

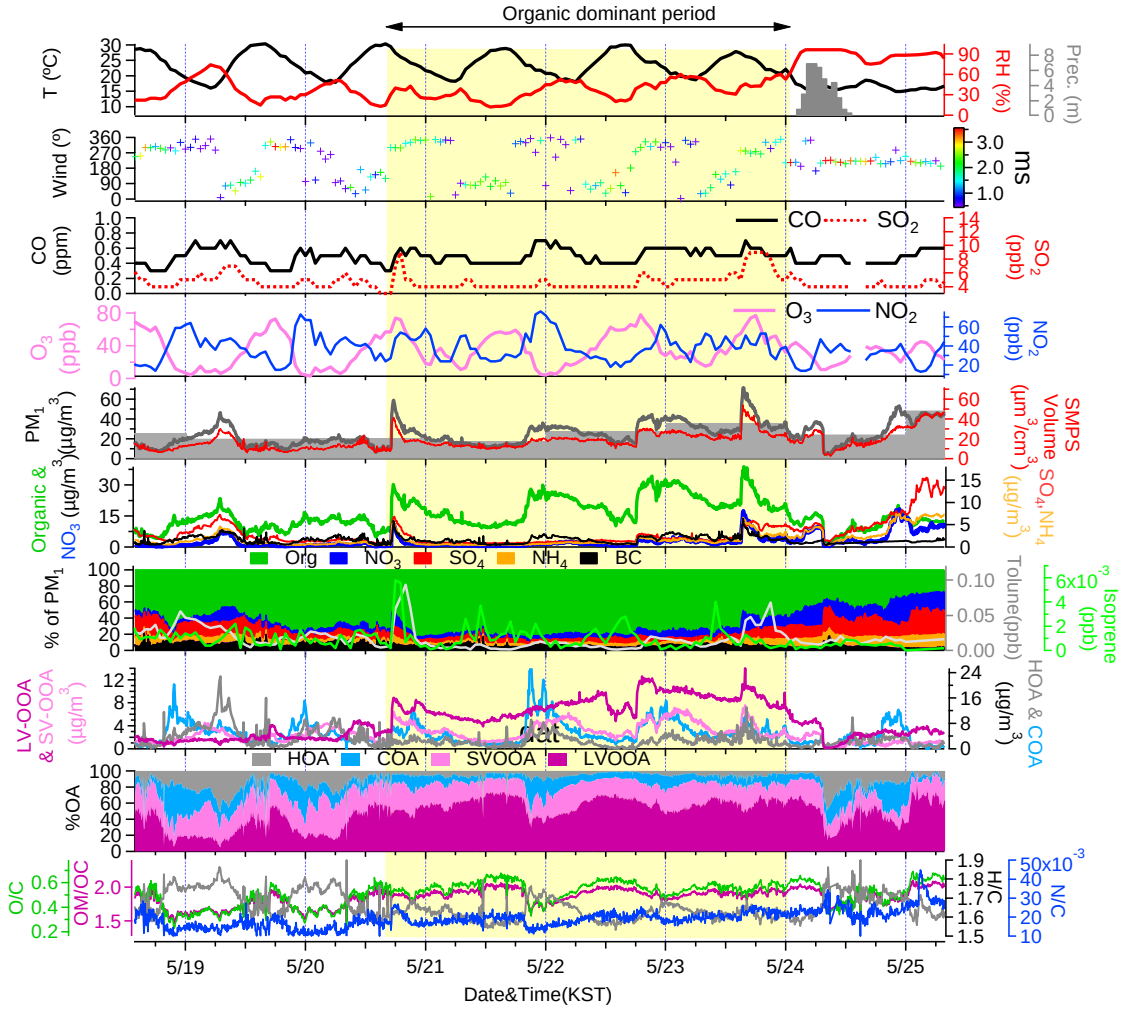

450

451 **Figure S20.** Overview of the temporal variations of submicron aerosols at the Korea Institute of
452 Science and Technology (KIST) in SMA from May 19 to May 25 including organic dominant
453 period colored by yellow (May 20, 17:00-May 24:0:00): **(a)** Time series of ambient air
454 temperature (T), relative humidity (RH), and precipitation (Precip.); **(b)** Time series of wind
455 direction (WD), with colors showing different wind speeds (WS); **(c)** Time series of CO and
456 SO_2; **(d)** Time series of O_3, and NO_2; **(e)** Time series of total particulate matter (PM_1), scanning
457 mobility particle sizer (SMPS) volume concentrations and also shown are the 24 h averaged
458 PM_1+BC with bars. **(f)** Time series of the organic (Org.), nitrate (NO_3^-), sulfate (SO_4^{2-}) ,
459 ammonium (NH_4^+) and BC aerosols; **(g)** Time series of the mass fractional contribution of
460 organic aerosols (Org.), nitrate (NO_3^-), sulfate (SO_4^{2-}), ammonium (NH_4^+), chloride (Cl^-), and BC
461 to total PM_1 together with isoprene and toluene time series; **(h)** Time series of each factor

462 derived from the positive matrix factorization (PMF) analysis; **(i)** Time series of the mass
463 fractional contribution to total organic aerosol (OA); (j) organic matter to organic carbon
464 (OM/OC), oxygen to carbon (O/C), hydrogen to carbon (H/C) and nitrogen to carbon (N/C)
465 (Canagaratna et al., 2015).
466
467
468
469
470
471
472
473
474
475
476
477
478
479
480
481
482
483
484
485
486

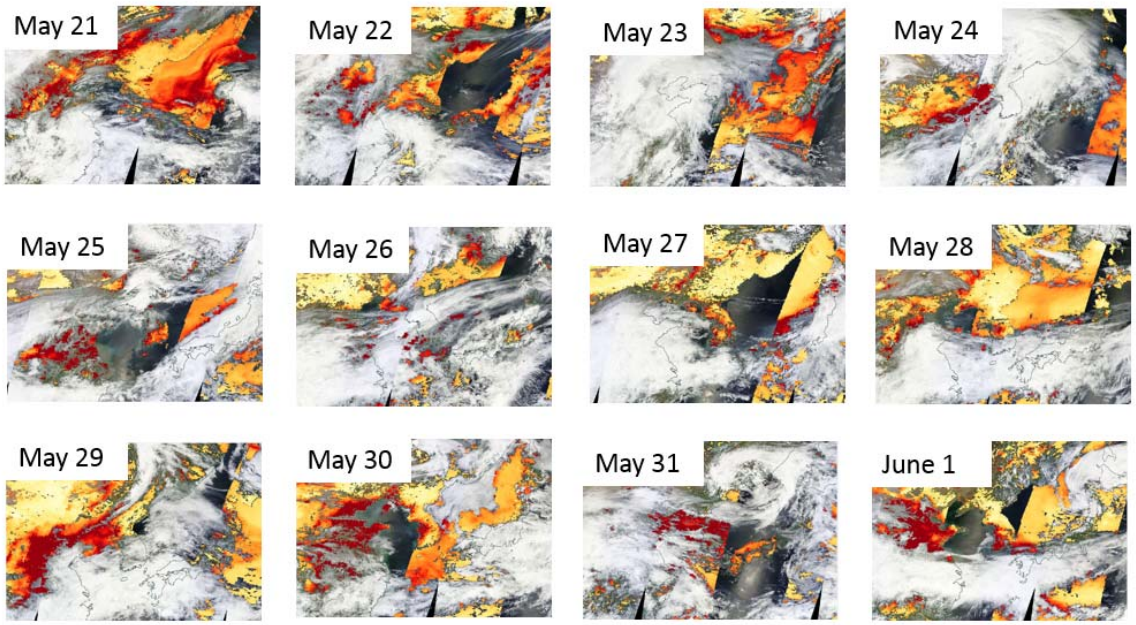

Figure S21. Long range transportation of plums from China to Korea during Haze period. Plots are from MODIS, terra.

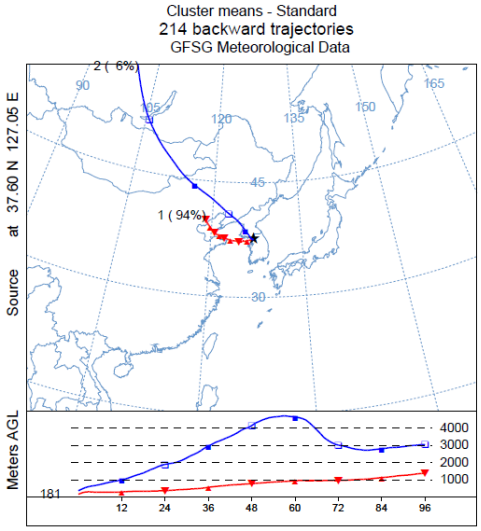

Figure S22. Two cluster solution of backtrajectroy analysis during haze period from (5/24 7:00-6/2 24:00). The trajectories were released at half of the mixing height at the KIST (latitude: 37.60N; longitude: 127.05E) and the average arriving height for the back trajectories for this study was approximately 181 m.

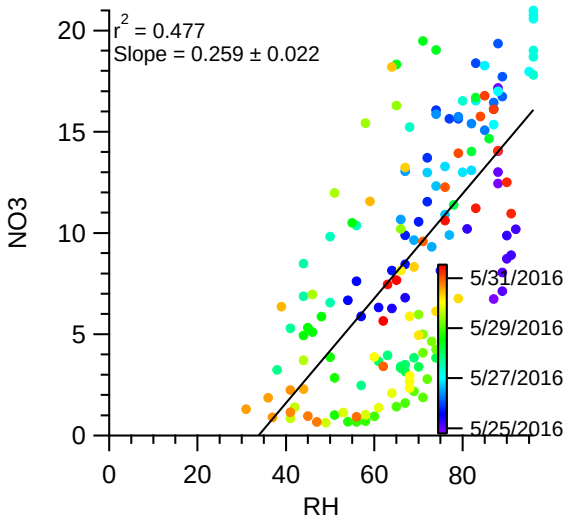

Figure S23. Scatterplots between nitrate vs. RH during haze period.

References

Aiken, A. C., Decarlo, P. F., Kroll, J. H., Worsnop, D. R., Huffman, J. A., Docherty, K. S., Ulbrich, I. M., Mohr, C., Kimmel, J. R., Sueper, D., Sun, Y., Zhang, Q., Trimborn, A., Northway, M., Ziemann, P. J., Canagaratna, M. R., Onasch, T. B., Alfarra, M. R., Prevot, A. S. H., Dommen, J., Duplissy, J., Metzger, A., Baltensperger, U., and Jimenez, J. L.: O/C and OM/OC ratios of primary, secondary, and ambient organic aerosols with high-resolution time-of-flight aerosol mass spectrometry, Environmental Science & Technology, 42, 4478-4485, 10.1021/es703009q, 2008.

Canagaratna, M. R., Jimenez, J. L., Kroll, J. H., Chen, Q., Kessler, S. H., Massoli, P., Hildebrandt Ruiz, L., Fortner, E., Williams, L. R., Wilson, K. R., Surratt, J. D., Donahue, N. M., Jayne, J. T., and Worsnop, D. R.: Elemental ratio measurements of organic compounds using aerosol mass spectrometry: characterization, improved calibration, and implications, Atmospheric Chemistry and Physics, 15, 253-272, 10.5194/acp-15-253-2015, 2015.

Kim, H., Zhang, Q., Bae, G. N., Kim, J. Y., and Lee, S. B.: Sources and atmospheric processing of winter aerosols in Seoul, Korea: insights from real-time measurements using a high-resolution aerosol mass spectrometer, Atmos. Chem. Phys., 17, 2009-2033, 10.5194/acp-17-2009-2017, 2017.

Kuwata, M., Zorn, S. R., and Martin, S. T.: Using Elemental Ratios to Predict the Density of Organic Material Composed of Carbon, Hydrogen, and Oxygen, Environmental Science & Technology, 46, 787-794, 10.1021/es202525q, 2012.

Middlebrook, A. M., Bahreini, R., Jimenez, J. L., and Canagaratna, M. R.: Evaluation of Composition-Dependent Collection Efficiencies for the Aerodyne Aerosol Mass Spectrometer using Field Data, Aerosol Science and Technology, 46, 258-271, 10.1080/02786826.2011.620041, 2012.

Zhang, Q., Canagaratna, M. R., Jayne, J. T., Worsnop, D. R., and Jimenez, J. L.: Time- and size-resolved chemical composition of submicron particles in Pittsburgh: Implications for aerosol sources and processes, Journal of Geophysical Research-Atmospheres, 110, 10.1029/2004jd004649, 2005.